

# Extracting Myofibre Orientation from Micro-CT Images: An Optimisation Study

Haibo Ni<sup>1</sup>, Simon J. Castro<sup>1</sup>, Robert S Stephenson<sup>2</sup>, Jonathan C Jarvis<sup>2</sup>,  
Tristan Lowe<sup>3</sup>, George Hart<sup>4</sup>, Mark R Boyett<sup>4</sup>, Henggui Zhang<sup>1</sup>

<sup>1</sup>Biological Physics Group, University of Manchester, Manchester, UK

<sup>2</sup>Department of Musculoskeletal Biology, University of Liverpool, Liverpool, UK

<sup>3</sup>Henry Moseley X-ray Imaging Facility, University of Manchester, Manchester, UK

<sup>4</sup>Cardiovascular Research Group, University of Manchester, Manchester, UK

## Abstract

*Recent studies introduced intensity based structure tensor analysis to extract the myocardium structure from micro X-ray computed tomography (micro-CT) images. The implementation of this method is empirical and encounters difficulties in validating the results. In this study, we performed series of tests using structure tensor analysis on synthetic tissue wedges with predefined fibre orientations, optimised the parameters of the method and applied it to the micro-CT images of a rabbit ventricular tissue. The accuracy of the method with several derivative filters and various parameters was investigated by quantifying the error in estimation in inclination angles. A measure of coherence was implemented to assess the coherence and reliability of the extracted orientations. We introduced Gaussian noise to investigate the robustness of this method. Our results suggest that the derivative of Gaussian and optimised Sobel derivative filter have better and balanced performances with overall mean error around 4°. The scale parameters play an important role in securing the accuracy. The algorithm is resistant to Gaussian noise. Using this method the myofibre orientation was successfully extracted from the ventricular tissue wedge images of the rabbit heart.*

## 1. Introduction

Anisotropic myofibre architecture has a significant impact on electric wave propagation in the heart and is important in developing structurally detailed 3-D anatomical models of cardiac electrophysiology. Diffusion Tensor Magnetic Resonance Imaging (DT-MRI) and micro X-ray computed tomography (micro-CT) are two non-invasive methods to acquire such information [1-3]. Compared with DT-MRI, micro-CT has advantages in the ultimate resolution and scanning efficiency [1, 4]. Unlike DT-MRI where the fibre orientation is acquired from the diffusion tensor, the structural information was

calculated using structure tensor analysis (STA) [1] in micro-CT. Though STA has been extensively applied to extract fibre-like features [2, 5], and the myofibres [6], its implementation is still empirical as there are no guidelines for choosing the scale parameters and derivative filters, two crucial aspects to be considered in the algorithm. Besides, it is a big challenge to validate extracted myofibre structure, as the true nature of myofibre structure is still an on-going debate [7].

To address this issue, we constructed synthetic tissue wedges with predefined fibre orientation to test the algorithm, and compared the performances of several derivative filters (DF): the finite difference method (FDM), the Sobel derivative filter (SDF) and its optimised version (OPSDF), derivative of Gaussian (DoG) [8] and Farid & Simoncelli derivative (FSD) [9]. The role of scale parameters in their performances was investigated. Gaussian noise was added to study the robustness of the algorithm and derivative filters. The algorithm was applied to a micro-CT scanned rabbit ventricular tissue wedge to extract the fibre orientations.

## 2. Methods

The principle of STA has been introduced in detail previously [5]. Briefly, an image volume  $f(\mathbf{x})$ , the scale space representation is defined as:

$$L(\mathbf{x}, t) = g(\mathbf{x}, t) * f(\mathbf{x}) \quad (1)$$

where  $g(\mathbf{x}, t)$  is the Gaussian kernel with inner scale  $t$ . The structure tensor is given by:

$$\mathbf{J}(\mathbf{x}, t, \rho) = g(\mathbf{x}, \rho) * \begin{pmatrix} L_{x1}^2 & L_{x1}L_{x2} & L_{x1}L_{x3} \\ L_{x2}L_{x1} & L_{x2}^2 & L_{x2}L_{x3} \\ L_{x3}L_{x1} & L_{x3}L_{x2} & L_{x3}^2 \end{pmatrix} \quad (2)$$

where  $g(\mathbf{x}_0, \rho)$  is another Gaussian filtering kernel with outer scale  $\rho$ , and  $L_{xi}$  denotes the image gradient. The orientation  $\mathbf{v}$  can be solved through eigen-value analysis. The fibre is found where  $\lambda_1 \approx \lambda_2 \gg \lambda_3 \geq 0$ , and  $\mathbf{v}$  is the eigenvector corresponding to  $\lambda_3$  [5].

To represent the coherence and reliability of the estimated local fibre orientations, a coherence measurement for a given scale  $s$ , is defined as [10]:

$$Coh(s) = (1 - \exp(-8 \frac{\lambda_2^2}{\lambda_1^2})) \exp(-2 \frac{\lambda_3^2}{\lambda_1 \lambda_2}) (1 - \exp(-\frac{\|\mathbf{J}\|_F^2}{\|\mathbf{J}\|_{\max}^2})) \quad (3)$$

Synthetic tissue wedges (STW) consisting of artificial fibres with predefined inclination angles were constructed (Figure 1), in which we used 1 to denote the intensity of the pixels on a fibre and 0 for the non-fibre pixels. The fibres within a single sheet shared the same inclination angle while the transverse angles were fixed to  $90^\circ$ . The structural parameters of the tested STWs are shown in Table 1. The errors were quantified as the deviations of the computed angles from the predefined ones.

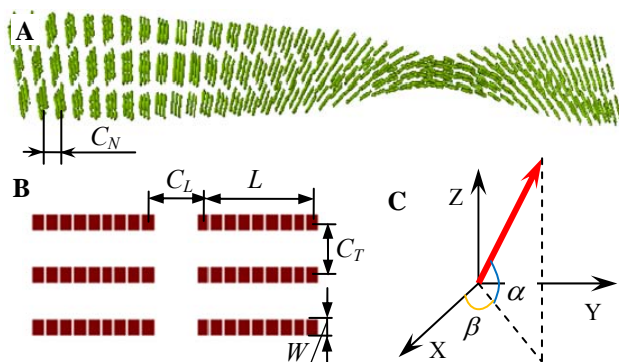


Figure 1. Predefined fibre structure and its structural parameters. (A) Synthetic tissue wedge with varying inclination angles. (B) Fibres within a tissue sheet. The structural parameters are as follows:  $C_N$  (normal clearance between the sheets),  $C_L$  (longitudinal clearance),  $C_T$  (transversal clearance),  $L$  (length of the fibre),  $W$  (width of the fibre). (C) Definition of fibre orientation angles:  $\alpha$  (inclination angle),  $\beta$  (transverse angle).

Table 1. Structural parameters of the testing STWs.

STW	$C_N$	$C_L$	$C_T$	$W$	$L$
Single fibre pattern (SFP)	2	-	-	1	33
Parallel continuous fibre pattern (CFP)	2	-	2	1	33
Parallel discontinuous fibre pattern (DCFP)	2	2	2	1	5

### 3. Results

#### 3.1. Performance of derivative filters

The algorithm was first applied to the simplest fibre pattern: only one long fibre within a tissue sheet (SFP, see Table 1). FSD was used to approximate the gradients. The resultant vectors are shown in Figure 2. The extracted vectors are consistent with the predefined orientations, except for those at the ends of the fibres, where the computed vectors are perpendicular to the real direction.

As the errors are dependent on the pixel position on the fibre, both errors at the centre pixel of fibres ( $E_{CP}$ ) and average errors of all on-fibre-pixels on the same sheet ( $AE_{OFP}$ ) were quantified.  $E_{CP}$  is a better error indicator as most pixels away from the fibre ends share the same error with the centre pixel of the fibre. In this simple case, the algorithm with FSD yielded ideal accuracy in estimating inclination angles, with  $E_{CP}$  less than  $0.6^\circ$ . The transverse angles were found to be uniformly  $90^\circ$ . Therefore, the following tests were focused on the inclination angles.

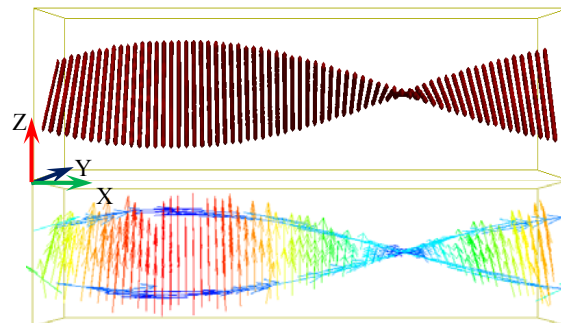


Figure 2. Comparison between STW (upper panel) and extracted fibre orientations (bottom panel) by FSD. The scale parameters were:  $t = 0.60$  and  $\rho = 0.95$ .

The parallel fibres (CFP and DCFP, see Table 1) were constructed to allow for further tests as well as comparing the performance of each of the DFs. Both  $E_{CP}$  and  $AE_{OFP}$  using the five DFs were quantified for the two fibre patterns with the same parameters ( $t = 0.60$  and  $\rho = 0.95$ ). The results are shown in Figure 3. The performance of the algorithm varies largely among the DFs for different fibre patterns. Generally, the algorithm exhibited better performance on the CFP, and  $AE_{OFP}$  is larger than  $E_{CP}$ , largely due to larger errors at fibre ends. The dependence of the error on the predefined angles indicates the rotation-variance of the derivatives (FDM, SDF). The FSD rendered distinct performances between the two fibre patterns, with mean  $E_{CP}$  less than  $1^\circ$  on the CFP, while the computed directions almost perpendicular to the predefined orientations on the DCFP. The FDM yielded errors as large as  $15^\circ$  on the two fibre patterns. The SDF performed better, with mean  $E_{CP}$  around  $5^\circ$  in both cases. OPSDF and DoG both exhibited balanced performances on the CFP and DCFP with mean  $E_{CP}$  within  $2^\circ$  and  $AE_{OFP}$  around  $4^\circ$  on CFP and  $8^\circ$  on DCFP, though DoG imposed larger errors at fibre ends (higher  $AE_{OFP}$ ). The results suggest that FSD performed well in the regular and continuous fibres, whereas OPSDF and DoG show higher robustness processing discontinuous fibres.

#### 3.2. The role of the smoothing scales

Application of the two Gaussian smooth kernels is important in implementing the algorithm, as its accuracy

was found to be scale-dependent. We calculated the mean errors and coherencies with varying scales from 0 (without Gaussian kernel) to 2. Results are shown in Figure 4. Tests on the CFP suggest that the derivatives allow for wide range of scales, though the outer scales should be greater than 0.2, and for FSD  $\rho$  should be over 0.9 when  $t > 1.5$ , in order to secure the accuracy in angle estimations. Error tests on the DCFP indicate the proper use of the scales is crucial to secure accuracy under such conditions, where the acceptable scale ranges are approximately  $\{t < 0.9, \rho > 0.2\}$  for OPSDF and DoG, and  $\{t < 0.5, 0.9 > \rho > 0.4\}$  for FSD. This is consistent with Figure 3. Figure 4C shows the coherence (defined in eqn. (3)) measured corresponding to Figure 4B. The coherence response has larger values at optimal scales, referring to lower error areas in Figure 4B, demonstrating the competence of the coherence measurement.

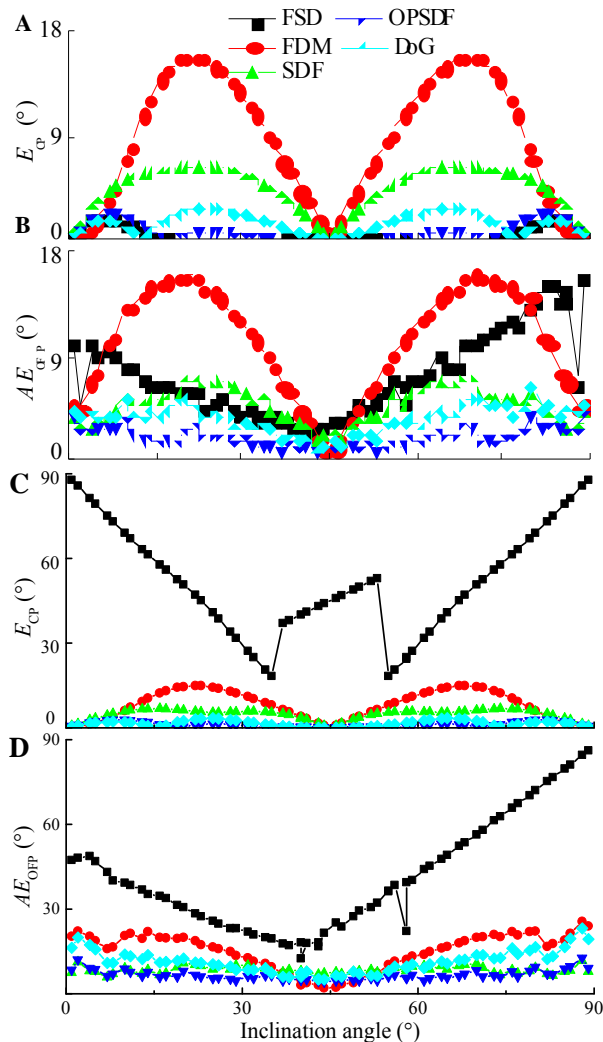


Figure 3. Averaged errors in inclination angles with respect to the predefined inclination angles.  $E_{CP}$  (A, C) and  $AE_{OFF}$  (B, D) with the fibre patterns CFP (A, B) and DCFP (C, D).

### 3.3. Effects of the image noise

The performance of the algorithm with image noise was examined by adding the Gaussian noise to the STW. Optimised scale parameters according to Figure 4 were applied ( $t = 0.30, \rho = 0.75$ ). Results are shown in Figure 5. The extracted orientation accuracy is diminished with the increase of noise. OPSDF and DoG exhibited comparable performances, securing good accuracies with image noise level at ( $m \leq 0.6, \sigma^2 = 0.01$ ) or ( $m = 0.5, \sigma^2 \leq 0.02$ ). Again, performance of FSD was not as competent, yielding larger errors and dependence on the noise.

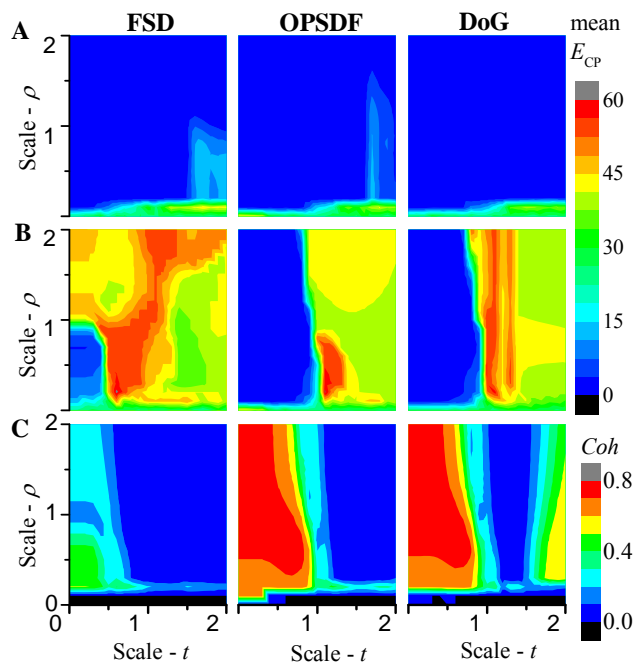


Figure 4. Dependence of mean error and coherence at the centre pixels on the smoothing scales. (A) Mean  $E_{CP}$  tests on the CFP. (B) Mean  $E_{CP}$  tests on the DCFP. (C) Coherence response tests on the DCFP.

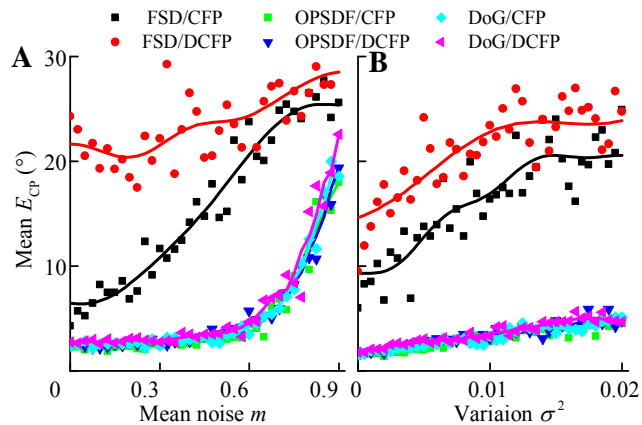


Figure 5. Mean  $E_{CP}$  with respect to Gaussian noises. (A)  $\sigma^2 = 0.01$ . (B)  $m = 0.5$ .

### 3.4. Implementation on the tissue images

The algorithm was implemented to extract fibre orientations from micro-CT images of a rabbit heart. The DoG was used to construct the structure tensor, which was then down-sampled once. The scale parameters were:  $t = 1.2$  and  $\rho = 1.25$ . Figure 6 shows the extracted smooth myocardium and the thin Purkinje fibre (PF) inside the ventricular chamber. The fibre orientation gradually changes from the epicardium (EPI) to the endocardium (ENDO), showing a transmural heterogeneity. Our results are consistent with the work by Plank *et al.* [2].

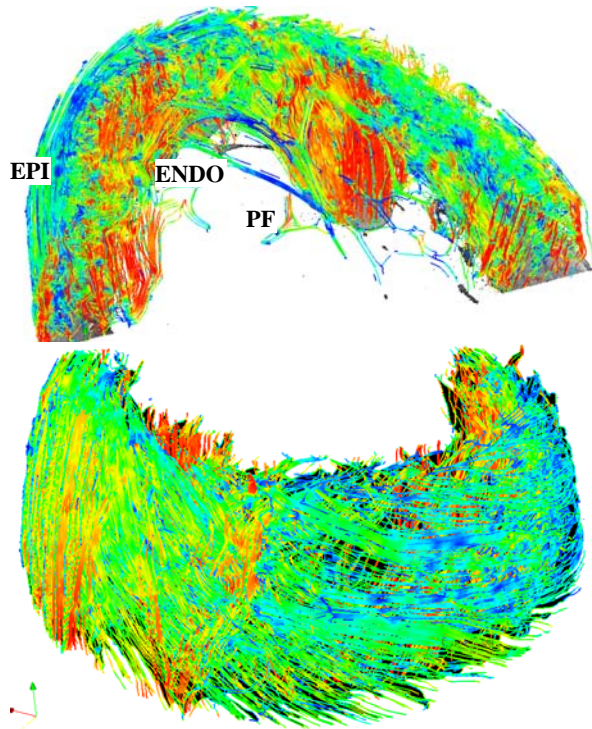


Figure 6. Extracted fibre from a rabbit ventricular tissue wedge, the colour corresponds to the inclination angles.

## 4. Discussion and conclusion

Implementation of the STA suggests that the algorithm is competent in extracting the myofibres, given that proper derivatives and smoothing scales are applied. However, our data suggests that FDM yielded large errors in angle estimation; as such its use in STA is dubious. Though better than FDM, SDF is not competent either. Whilst FSD performs best out of all DFs when the fibres are regular and continuous, its accuracy is largely subject to image quality and choice of scales, and the estimated orientations at the boundaries of fibres may not be reliable. OPSDF and DoG are recommended with balanced performances and overall errors around  $4^\circ$  in general cases.

The proper use of smoothing scales is important in

securing accuracy of angle estimations. The implemented coherence measurement is a good representation of the reliability of the extracted orientations, showing potentials to be used as an indicator in automatic scale selection. The algorithm using DoG and OPSDF rendered good resistance to Gaussian noises. The implementation of the algorithm on the micro-CT images indicates its competence in extracting myofibre orientations.

## Acknowledgements

This work was supported by EPSRC and BHF.

## References

- [1] Aslanidi OV, et al. Application of micro-computed tomography with iodine staining to cardiac imaging, segmentation, and computational model development. *IEEE Trans Med Imaging* 2013;32:8-17.
- [2] Plank G, et al. Generation of histo-anatomically representative models of the individual heart: tools and application. *Philos Trans A Math Phys Eng Sci* 2009; 367:2257-92.
- [3] Helm P, Beg MF, Miller MI, and Winslow RL. Measuring and mapping cardiac fiber and laminar architecture using diffusion tensor MR imaging. *Ann N Y Acad Sci* 2005; 1047:296-307.
- [4] Stephenson RS, Boyett MR, et al. Contrast enhanced micro-computed tomography resolves the 3-dimensional morphology of the cardiac conduction system in mammalian hearts. *PLoS One* 2012;7(4):e35299.
- [5] Krause M, Hausherr JM, et al. Determination of the fibre orientation in composites using the structure tensor and local X-ray transform. *Journal of Materials Science* 2010; 45:888-896.
- [6] Zhao J, Butters TD, et al. Image-based model of atrial anatomy and electrical activation: a computational platform for investigating atrial arrhythmia. *IEEE Trans Med Imaging* 2013;32:18-27.
- [7] Gilbert SH, Benson AP, et al. Regional localisation of left ventricular sheet structure: integration with current models of cardiac fibre, sheet and band structure. *Eur J Cardiothorac Surg* 2007;32:231-49.
- [8] Jähne B. *Digital image processing [Electronic book]*, 6th rev. and ext. ed. Berlin; New York: Springer, 2005.
- [9] Farid H, Simoncelli EP. Differentiation of discrete multidimensional signals. *IEEE Transactions on Image Processing* 2004;13:496-508.
- [10] Frangi AF, Niessen WJ, et al. Multiscale vessel enhancement filtering. *Medical Image Computing and Computer-Assisted Intervention - Miccai'98* 1998;1496: 130-137.

Address for correspondence.

Haibo Ni,  
Biological Physics Group,  
University of Manchester  
M13 9PL, UK  
[Haibo.ni@postgrad.manchester.ac.uk](mailto:Haibo.ni@postgrad.manchester.ac.uk)